Research Article Vol. 35, No. 10 / October 2018 / Journal of the Optical Society of America A 1705

Journal of the Optical Society of America A
OPTICS, IMAGE SCIENCE, AND VISION

Correcting flat mirrors with surface stress: analytical stress fields

Brandon D. Chalifoux,[1] Ralf K. Heilmann,[2] and Mark L. Schattenburg[2,*]

[1]Department of Mechanical Engineering, Massachusetts Institute of Technology, 77 Massachusetts Ave., Cambridge, Massachusetts 01803, USA
[2]Kavli Institute for Astrophysics and Space Science, Massachusetts Institute of Technology, 70 Vassar St., Cambridge, Massachusetts 01803, USA
*Corresponding author: marks@space.mit.edu

Received 21 May 2018; revised 26 August 2018; accepted 26 August 2018; posted 27 August 2018 (Doc. ID 331878); published 17 September 2018

Thin mirrors, important for next-generation space telescopes, are difficult to accurately fabricate. One approach is to fabricate a mirror using traditional methods, then to bend the mirror using surface stress to correct residual height errors. We present two surface stress fields that correct any height error field in thin flat plates. For round plates, we represent these as linear combinations of Zernike polynomials. We show that equibiaxial stress, a common and easy-to-generate state of stress, cannot generally be used to make exact corrections. All three components of the surface stress are needed for exact corrections. We describe a process to design an equibiaxial stress field to make approximate corrections in round plates. Finally, we apply the three stress fields to simulate flattening of a measured glass wafer with 3.64 μm root-mean-squared (RMS) height error. Using our chosen equibiaxial stress field, the residual error is 0.34 μm RMS. In comparison, using all three stress components, the correction is exact and the required RMS stress is about 2.5× smaller than when using equibiaxial stress only. We compare the deformation with a finite element model and find agreement within 10 nm RMS in all three cases.

OCIS codes: (220.1080) Active or adaptive optics; (310.6845) Thin film devices and applications; (350.1260) Astronomical optics.

https://doi.org/10.1364/JOSAA.35.001705

1. INTRODUCTION

Thin mirrors have been used in space telescopes [1] and concentrated solar thermal systems [2] and are being considered for a number of space telescope mission concepts (e.g., [3,4]). Obtaining high optical quality of thin mirrors is a challenge because thin mirrors deform easily during fabrication. Existing finishing methods such as ion-beam figuring (IBF) and magneto-rheological finishing (MRF) can in some cases be used to correct surface height errors in thin mirrors, but must be used prior to depositing reflective coatings, which can deform thin substrates significantly. In addition, for very low spatial-frequency errors, the height error of a mirror can be many micrometers, which requires a long time to remove.

Stress-based correction, in which stress is applied to the surface of a substrate to bend the substrate and cause a desired deformation, is an alternative approach to correcting height errors in thin mirrors, and is particularly well-suited to correcting low spatial-frequency errors. Many passive and active approaches have been developed for applying surface stress to cause a desired deformation in a plate or membrane [4–13]. For example, ion implantation [10] applies a static correction, while deformable mirrors apply active correction [5,6].

The primary purpose of this paper is to answer the following question: what stress fields could be applied to the surface to achieve a desired deformation field? We will primarily address this question analytically, and to simplify the problem, we limit our analysis to thin, nearly flat plates. However, the results presented here serve as a good starting point for correcting thin shells (curved plates).

Every method of deforming a mirror using surface stress relies on the same basic mechanism: an internal strain is generated in a thin film on a much thicker plate, as illustrated in Fig. 1. Since the thin film is laterally constrained by the plate, in-plane stress develops in the film. The plate-film system reaches static equilibrium by deforming (primarily bending). If the stress field in the film can be controlled, then the deformation field can also be controlled and could be chosen to cancel any surface height errors in the mirror. While in general a stress tensor has six independent components, only the three in-plane components of stress in the film contribute significantly to deformation of the plate, provided the film is thin compared to the plate thickness. Thus, the film stress consists of two normal stress components and one shear stress component.

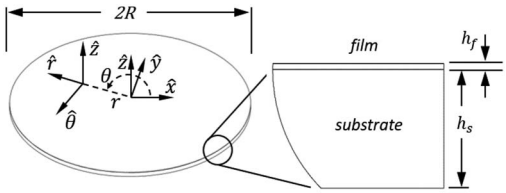

Fig. 1. Plate-film system geometry. Cartesian and polar coordinate system unit vectors are each shown.

An equibiaxial stress state is where both of the in-plane normal stress components are equal and the shear stress component is zero. An equibiaxial stress state and a general stress state are illustrated in Fig. 2. Many methods being studied, such as using piezoelectric films with plane electrodes [4,7,8] and adjusting film stress during deposition [9], are typically limited to controlling equibiaxial stress. We will show that, when no external loads are applied to the mirror, this limits the types of surface errors that may be exactly corrected. Several methods are being studied that allow at least some control of all three components of the film stress. Examples include using ion implantation [10], magnetostrictive films [11], patterned films [12], or piezoelectric films with inter-digitated electrodes [13]. Designing a system to adequately control the three components of film stress is more complex than controlling only equibiaxial stress. However, we will show that, in general, exact corrections (within the limits of our assumptions) are only possible if all three components of surface stress are controlled.

The deformation of the plate-film system is proportional to the stress in the film multiplied by the film thickness, referred to in the present work as the integrated stress. The integrated stress is a tensor field with three components (see Fig. 2). For a uniform integrated stress field, a uniform change in curvatures results and may be calculated by Stoney's equation [14] for an equibiaxial stress state and the equation by Suresh and Freund [15] for a general stress state.

For non-uniform, equibiaxial, and general integrated stress fields, much work has been published [11,16–18]. Ngo *et al.* [16] considered equibiaxial stress to generate a displacement field, which we will show is insufficient to generate an arbitrary displacement field. Huang *et al.* [17] found that there is not a unique stress field to generate an arbitrary displacement field, and so presented stress fields for only two specific displacement fields. We present two stress fields that generate any displacement field on a flat plate. To our knowledge, a stress field that generates an arbitrary displacement field has not been presented before.

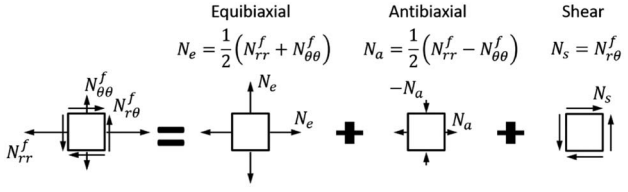

Fig. 2. Representation of the plane stress state in a differential element used in the present work.

There are also several methods of numerically calculating a stress field that generates a desired displacement field. These have been primarily applied to deformable mirrors. The most common method is to calculate or measure a set of actuator influence functions (the deformation field caused by each actuator) and to use a pseudoinverse to minimize the least-squared error between the target and desired surface shape [19]. A similar method has been used for continuous equibiaxial stress distributions on mirrors [20]. Numerical methods, however, do not provide as much insight as analytical approaches.

Optical surface height errors are commonly described using Zernike polynomials, a set of functions that are mutually orthonormal over a unit disk [21]. We will represent the integrated stress field as a linear combination of Zernike polynomials, using the work of Janssen [22] and Noll [23]. We will also describe a method to design a stress field that provides an approximate correction, when we are restricted to using only the equibiaxial component. This process balances the residual surface height and the required stress magnitude.

The analysis of this work is intended to be agnostic to the method of applying stress, and we do not address the specific limitations of each method. In practical applications, actuators are sometimes spatially discretized, integrated stress magnitudes are limited, and not all stress states may be accessible. These limitations, in addition to error sources such as metrology or stress location and magnitude, will tend to degrade performance compared to the results presented here. For active correction, mirrors are usually corrected after mounting, and the mount may apply additional loads on the mirror. In many cases, practical applications will require computational approaches to account for these details (among others), but the stress fields presented serve as a starting point for further optimization and provide intuition useful for further development of the various methods of applying stress-based correction.

2. PROBLEM FORMULATION

We consider a nearly flat, thin round plate with a significantly thinner stressed film bonded to one surface with no external loads. This system is illustrated in Fig. 1. The plate has a surface height error field $w_e(r,\theta)$ that is small compared to the substrate thickness. We would like to generate a displacement, $w(r,\theta) = -w_e(r,\theta)$, to correct the height errors in the plate.

Our goal is to determine the stress field that must be applied by the film to correct the height error. In general, the stress field will have three components: two normal stress components and one shear stress component. All three are assumed to be controllable, without any magnitude limit. We also assume that the film stress is continuous, not discretized (as is typical for active correction). We make the following kinematic and geometric assumptions to simplify this problem:

- The film thickness is small compared to the substrate thickness ($h_f \ll h_s$).
- The substrate thickness is constant and small compared to the substrate radius ($h_s \ll R$).

• The deformation and initial surface height fields are small compared to the thickness of the substrate ($w \ll h_s$).
• The film and substrate are linear elastic, isotropic, and homogeneous.
• The film's elastic modulus and Poisson's ratio are the same as those of the substrate.

A. Governing Equation

Several authors, such as Huang *et al.* [17] and Wang *et al.* [11], have derived, in detail, the governing equations for a thin stressed film on a round and rectangular plate, respectively. Here we outline a simple derivation that ignores any effect of displacement on the film stress; the strain in the film due to substrate bending is assumed to be small compared to the original internal strain that causes the film stress. This is a valid assumption for thin films, and indeed we obtain the same governing equation as Huang *et al.*

The net bending moments acting on the substrate are

$$M^N_{\alpha\beta} = M_{\alpha\beta} - \frac{h_s}{2} N^f_{\alpha\beta}, \tag{1}$$

where $\{\alpha, \beta\} = \{r, \theta\}$ in polar coordinates, $M^N_{\alpha\beta}$ is the net bending moment acting in the $\alpha\beta$ direction, $M_{\alpha\beta}$ is the internal bending moment from the substrate, and $N^f_{\alpha\beta}$ is the integrated stress of the film in the $\alpha\beta$ direction. For a thin plate, the Kirchhoff–Love plate theory (e.g., Ref. [24]) provides a good approximation of the plate deformation. As in the Kirchhoff–Love plate theory, the midplane substrate curvatures are related to the internal bending moments by

$$M_{\alpha\beta} = D[(1-\nu_s)\kappa_{\alpha\beta} + \delta_{\alpha\beta}\nu_s(\kappa_{rr} + \kappa_{\theta\theta})], \tag{2}$$

where $\delta_{ij} = \begin{cases} 1 & \text{if } i = j \\ 0 & \text{if } i \neq j \end{cases}$ is the Kronecker delta function. The plate stiffness is $D = E_s(h_s + h_f)^3/12(1-\nu_s^2)$ as normally defined in the Kirchhoff–Love plate theory, E_s is the substrate elastic modulus, and ν_s is the substrate Poisson's ratio. For a thick film with elastic constants significantly larger than the substrate, D may be modified as in Ref. [15]. The curvatures, in polar coordinates, are defined as $\kappa_{rr} = \frac{\partial^2 w}{\partial r^2}$, $\kappa_{\theta\theta} = \frac{1}{r}\frac{\partial w}{\partial r} + \frac{1}{r^2}\frac{\partial^2 w}{\partial \theta^2}$, and $\kappa_{r\theta} = \frac{\partial}{\partial r}\left(\frac{1}{r}\frac{\partial w}{\partial \theta}\right)$.

The static equilibrium of a differential element of the plate-film system results in

$$\frac{\partial^2 M^N_{rr}}{\partial r^2} + \frac{2}{r}\frac{\partial M^N_{rr}}{\partial r} + \frac{1}{r^2}\frac{\partial^2 M^N_{\theta\theta}}{\partial \theta^2} - \frac{1}{r}\frac{\partial M^N_{\theta\theta}}{\partial r} + \frac{2}{r}\frac{\partial^2 M^N_{r\theta}}{\partial r \partial \theta} + \frac{2}{r^2}\frac{\partial M^N_{r\theta}}{\partial \theta} = 0. \tag{3}$$

The plate-film system has free edges as boundary conditions. At edge ($r = R$), therefore, the net radial moment M^N_r is zero [Eq. (4a)] and the net effective shear force V^N_r is zero [Eq. (4b)]:

$$[M^N_{rr}]_{r=R} = 0, \tag{4a}$$

$$[V^N_r]_{r=R} = -\left[\frac{\partial M^N_{rr}}{\partial r} + \frac{M^N_{rr} - M^N_{\theta\theta}}{r} + \frac{2}{r}\frac{\partial M^N_{r\theta}}{\partial \theta}\right]_{r=R} = 0. \tag{4b}$$

We represent the integrated stress field components as equibiaxial, antibiaxial, and shear components (Fig. 2), defined as $N_e = \frac{1}{2}(N^f_{rr} + N^f_{\theta\theta})$, $N_a = \frac{1}{2}(N^f_{rr} - N^f_{\theta\theta})$, and $N_s = N^f_{r\theta}$. The equilibrium equation and boundary conditions may be expressed as functions of the curvatures and integrated stress components $\{N_e(r,\theta), N_a(r,\theta), N_s(r,\theta)\}$ to become the governing equation [Eq. (5a)] and boundary conditions [Eqs. (5b) and (5c)]:

$$\nabla^2 N_e + \left(\frac{\partial^2 N_a}{\partial r^2} + \frac{3}{r}\frac{\partial N_a}{\partial r} - \frac{1}{r^2}\frac{\partial^2 N_a}{\partial \theta^2}\right) + \left(\frac{2}{r}\frac{\partial^2 N_s}{\partial r \partial \theta} + \frac{2}{r^2}\frac{\partial N_s}{\partial \theta}\right) = \frac{2D}{h_s}\nabla^2(\kappa_{rr} + \kappa_{\theta\theta}), \tag{5a}$$

$$[N_e + N_a]_{r=R} = \frac{2D}{h_s}[\kappa_{rr} + \kappa_{\theta\theta} - (1-\nu_s)(\kappa_{\theta\theta})]_{r=R}, \tag{5b}$$

$$\left[\frac{\partial N_e}{\partial r} + \frac{\partial N_a}{\partial r} + \frac{2}{r}N_a + \frac{2}{r}\frac{\partial N_s}{\partial \theta}\right]_{r=R} = \frac{2D}{h_s}\left[\frac{\partial}{\partial r}(\kappa_{rr} + \kappa_{\theta\theta}) + (1-\nu_s)\frac{1}{r}\frac{\partial \kappa_{r\theta}}{\partial \theta}\right]_{r=R}. \tag{5c}$$

B. Limitation of Equibiaxial Stress

In the next section we present two integrated stress fields $\{N_e(r,\theta), N_a(r,\theta), N_s(r,\theta)\}$ that generate a desired displacement field $w(r,\theta)$. Before presenting these stress fields, we show that harmonic displacement fields cannot be generated using N_e only, and therefore equibiaxial stress alone is not sufficient to generate an arbitrary displacment field. This limitation will guide the derivation of Stress Field II in the next section.

A harmonic displacement field is defined here as a finite and continuous displacement field that satisfies Laplace's equation, $\nabla^2 w = \kappa_{11} + \kappa_{22} = 0$, such as a pure astigmatism (or saddle shape). The numerical curvature subscripts indicate orthogonal directions in any coordinate frame.

We assume that there is a non-zero harmonic displacement field. We show that if $N_a = N_s = 0$, there is no work done by the integrated stress field, and therefore there is no displacement, contradicting the non-zero displacement assumption. As in the development of the governing equation, we ignore the strain energy due to net in-plane forces in the substrate since they do not contribute to small out-of-plane deformations. For a flat plate of arbitrary shape with a stressed film, the total potential Π is the difference of the internal strain energy due to bending, U_b, and the work done by the integrated stress field, W_f:

$$\Pi = U_b - W_f = \frac{1}{2}\iint_S (M_{11}\kappa_{11} + M_{22}\kappa_{22} + 2M_{12}\kappa_{12})\mathrm{d}A - \frac{h_s}{2}\iint_S (N^f_{11}\kappa_{11} + N^f_{22}\kappa_{22} + 2N^f_{12}\kappa_{12})\mathrm{d}A. \tag{6}$$

When the system is in equilibrium, the variation of the total potential with respect to small arbitrary displacements is zero. We substitute the definitions of the net moments from Eq. (1)

and the integrated stress components from Fig. 2. The work done by external forces becomes

$$W_f = \frac{h_s}{2}\iint_S [N_e(\kappa_{11}+\kappa_{22}) + N_a(\kappa_{11}-\kappa_{22}) + 2N_s\kappa_{12}]\mathrm{d}A. \tag{7}$$

If $\kappa_{11}+\kappa_{22}=0$ and $N_a = N_s = 0$, then $W_f = 0$. There is no work done by external forces in this case and no deformation.

Vdovin *et al.* [18] point out that this can be alleviated by applying equibiaxial stress or forces outside of a "correction aperture," defined as the subset of the plate area that is used as an optical surface. This approach would be equivalent to applying forces and moments external to the plate.

This limitation of using equibiaxial stress only to correct the surface of flat mirrors is severe, in general. While equibiaxial stress cannot be used to make arbitrary exact surface height corrections, approximate corrections are possible and are described in Section 5.

3. INTEGRATED STRESS FIELD SOLUTIONS

In this section we present two integrated stress fields $\{N_e(r,\theta), N_a(r,\theta), N_s(r,\theta)\}$ that generate a desired displacement field $w(r,\theta)$. Since there is one governing equation and there are three independent variables, we do not expect there to be a unique solution. The two solutions we present are each useful in different situations. Stress Field I provides an exact solution (within the assumptions outlined in Section 2) for any flat plate shape, while Stress Field II is an exact solution for round plates only.

Stress field I requires larger root-mean-squared (RMS) non-equibiaxial stress components than Stress Field II. This may be important even for stress-based correction methods that are capable of applying non-equibiaxial stress. For example, ion implantation in glass is capable of generating significantly larger equibiaxial stress than non-equibiaxial stress [10].

Many methods of stress-based figure correction allow control of equibiaxial stress only. We showed in Section 2.B that displacement fields described by harmonic functions *cannot* be generated exactly with equibiaxial stress alone. Stress Field II is particularly useful for making approximate corrections using equibiaxial stress only.

In Section 4, we represent Stress Field II as a linear combination of Zernike polynomials, and we describe how to calculate the Zernike spectrum of Stress Field I. In Section 5, we describe a process to use Stress Field II to make approximate corrections using equibiaxial stress only. In Section 6, we use the three Stress Fields (Stress Fields I and II, and the Equibiaxial Only stress field) to simulate flattening of a measured glass wafer surface and compare the expected deformation with a finite element model.

A. Stress Field I

One obvious solution arises by combining Eqs. (1) and (2) and choosing the stress field components such that the net moments are zero (which also automatically satisfies the boundary conditions), resulting in

$$\begin{aligned} N_e &= \frac{D(1+\nu_s)}{h_s}(\kappa_{rr}+\kappa_{\theta\theta}),\\ N_a &= \frac{D(1-\nu_s)}{h_s}(\kappa_{rr}-\kappa_{\theta\theta}),\\ N_s &= \frac{D(1-\nu_s)}{h_s}2\kappa_{r\theta}. \end{aligned} \tag{8}$$

We may also transform both the curvature and stress tensor components into a Cartesian coordinate frame,

$$\begin{aligned} N'_e &= \frac{D(1+\nu_s)}{h_s}(\kappa_{xx}+\kappa_{yy}),\\ N'_a &= \frac{D(1-\nu_s)}{h_s}(\kappa_{xx}-\kappa_{yy}),\\ N'_s &= \frac{D(1-\nu_s)}{h_s}2\kappa_{xy}, \end{aligned} \tag{9}$$

where the curvatures are $\kappa_{xx} = \frac{\partial^2 w}{\partial x^2}$, $\kappa_{yy} = \frac{\partial^2 w}{\partial y^2}$, $\kappa_{xy} = \frac{\partial^2 w}{\partial x \partial y}$ and the stress components are $N'_e = \frac{1}{2}(N^f_{xx}+N^f_{yy})$, $N'_a = \frac{1}{2}(N^f_{xx}-N^f_{yy})$, $N'_s = N^f_{xy}$.

B. Stress Field II

In Section 2.B, we established that there are deformations that cannot be generated using equibiaxial stress only. In deriving Stress Field II, we separate the problem into three parts. First, we use equibiaxial stress only to attempt to correct the surface. Next, we determine the deformation error that results from this attempted correction. Finally, we use the non-equibiaxial stress components to correct this residual error.

The first part of this section derives the same equibiaxial stress as Ngo *et al.* [16]. However, they neither pointed out the resulting error nor offered a correction for that error, which we do later in this section.

We must make a distinction between the displacement field we aim to generate, $W(r,\theta)$, and the displacement field $w(r,\theta)$ that results from the application of the integrated stress field. The displacement and integrated stress field are assumed to be functions that are separable into radial and azimuthal parts,

$$\begin{aligned} w(r,\theta) &= \sum_{m=0}^{\infty} w^c_m(r)\cos\, m\theta + w^s_m(r)\sin\, m\theta,\\ W(r,\theta) &= \sum_{m=0}^{\infty} W^c_m(r)\cos\, m\theta + W^s_m(r)\sin\, m\theta,\\ N_i(r,\theta) &= \sum_{m=0}^{\infty} N^c_{i,m}(r)\cos\, m\theta + N^s_{i,m}(r)\sin\, m\theta, \end{aligned} \tag{10}$$

where $i = e, a, s$. We first solve the governing equation, Eq. (5), with $N_a = N_s = 0$ and $w = W$, to obtain the form of the integrated stress field that generates the desired deformation. The complete solution for N_e is the sum of the homogeneous solution and a particular solution:

$$N_e = \frac{2D}{h_s}\left[\nabla^2 W - \frac{1-\nu_s}{2R} \times \sum_{m=0}^{\infty}(1+\delta_{m0})(m+1)\left(\frac{r}{R}\right)^m \begin{pmatrix} a^c_m\cos m\theta \\ +a^s_m \sin m\theta \end{pmatrix}\right]. \tag{11}$$

Here, $a_m^{c,s}$ are constants to be determined from the boundary conditions (the dual superscript indicates either the cosine or sine term). The multipliers in the summation are added for later convenience.

The boundary conditions must be satisfied for w, not W. We must determine the deformation w that results from applying the stress field component N_e from Eq. (11). Finding the deformation $w(r,\theta)$ requires finding all functions $w_m^{c,s}(r)$. Each term is independent and must satisfy Eq. (5). We may integrate the stress field $N_{e,m}^{c,s}(r)$ by parts twice to find a particular solution and add to this the C^2-continuous and add the finite solutions to the biharmonic equation ($\nabla^4 w = 0$),

$$w_m^{c,s}(r) = \frac{h_s}{2D}\left[r^m \int_0^r \rho^{-2m-1}\left(\int_0^\rho \eta^{m+1} N_{e,m}^{c,s}(\eta)\mathrm{d}\eta\right)\mathrm{d}\rho\right] + c_m^{c,s} r^{m+2} - \begin{cases} \frac{R}{2m} b_m^{c,s}\left(\frac{r}{R}\right)^m & \text{if } m \geq 2 \\ 0 & \text{if } m < 2 \end{cases}. \tag{12}$$

We add constants in front of $b_m^{c,s}$ for later convenience. Note that for $m < 2$, an r^m term represents rigid-body motions. Since this plate has no external constraints, these rigid-body motions are undefined and we set them to zero. Using Eq. (11), we substitute a stress component, $N_{e,m}^{c,s}(r)$, into Eq. (12) to obtain

$$w - W = -\sum_{m=2}^{\infty} \frac{R}{2m}\left(\frac{r}{R}\right)^m (b_m^c \cos m\theta + b_m^s \sin m\theta) + \sum_{m=0}^{\infty} r^{m+2}\begin{bmatrix} \left(c_m^c - \frac{1+\delta_{m0}}{8R^{m+1}}(1-\nu_s)a_m^c\right)\cos m\theta \\ +\left(c_m^s - \frac{1+\delta_{m0}}{8R^{m+1}}(1-\nu_s)a_m^s\right)\sin m\theta \end{bmatrix}. \tag{13}$$

Since we choose the stress field constants $a_m^{c,s}$, we eliminate as much displacement error as possible by choosing $a_m^{c,s}/c_m^{c,s} = 8R^{m+1}/[(1+\delta_{m0})(1-\nu_s)]$. Using Eqs. (5b) and (5c), we may determine the constants, shown here for the cosine terms (for the sine terms, exchange cos for sin):

$$a_m^c = \left[\frac{dw_m^c}{dr} - \frac{m}{r}w_m^c\right]_{r=R} = \frac{1}{\pi}\int_{-\pi}^{\pi}\left[\frac{dw}{dr} - \frac{m}{r}w\right]\cos m\theta \mathrm{d}\theta,$$
$$b_m^c = \left[\frac{dw_m^c}{dr} + \frac{m}{r}w_m^c\right]_{r=R} = \frac{1}{\pi}\int_{-\pi}^{\pi}\left[\frac{dw}{dr} + \frac{m}{r}w\right]\cos m\theta \mathrm{d}\theta. \tag{14}$$

Note that, according to Eq. (12), $b_m^{c,s}$ is undefined for $m = 0, 1$, but if the average tip, tilt, and piston of a surface is zero, Eq. (14) results in $b_0^c = b_1^{c,s} = 0$. The height error $\Delta w(r,\theta)$ created by attempting to generate a surface height using Eq. (11) is

$$\Delta w(r,\theta) = w - W = -\sum_{m=2}^{\infty}\frac{R}{2m}\left(\frac{r}{R}\right)^m (b_m^c \cos m\theta + b_m^s \sin m\theta). \tag{15}$$

The residual height error is a harmonic displacement function and is therefore uncorrectable using an equibiaxial stress field (see Section 2.B). For a harmonic displacement field, Eq. (11) results in $N_e(r,\theta) = 0$ and $w(r,\theta) = 0$.

The residual error in Eq. (15) may be corrected using non-equibiaxial stress terms. We may solve the governing equation with $N_e = 0$ and $w = \Delta w(r,\theta)$ by assuming that N_a and N_s are of the form $N \propto (r/R)^k \cos m\theta$, where k is a positive integer.

The resulting solution for the antibiaxial and shear stress fields is

$$N_a = \frac{2D(1-\nu_s)}{h_s R}\sum_{m=2}^{\infty}\frac{m-1}{2}\left(\frac{r}{R}\right)^{m-2}\begin{pmatrix} b_m^c \cos m\theta \\ +b_m^s \sin m\theta \end{pmatrix},$$
$$N_s = \frac{2D(1-\nu_s)}{h_s R}\sum_{m=2}^{\infty}\frac{m-1}{2}\left(\frac{r}{R}\right)^{m-2}\begin{pmatrix} b_m^s \cos m\theta \\ -b_m^c \sin m\theta \end{pmatrix}. \tag{16}$$

The stress components of Eq. (16) are in polar coordinates, so the directions of the stress components change withposition on the surface relative to a fixed coordinate frame. We may represent these stress components in a Cartesian coordinate frame. The Cartesian stress components are defined in Section 3.A and are

$$N_a' = \frac{2D(1-\nu_s)}{h_s R}\sum_{m=2}^{\infty}\frac{m-1}{2}\left(\frac{r}{R}\right)^{m-2}\begin{pmatrix} b_m^c \cos(m-2)\theta \\ +b_m^s \sin(m-2)\theta \end{pmatrix},$$
$$N_s' = \frac{2D(1-\nu_s)}{h_s R}\sum_{m=2}^{\infty}\frac{m-1}{2}\left(\frac{r}{R}\right)^{m-2}\begin{pmatrix} b_m^s \cos(m-2)\theta \\ -b_m^c \sin(m-2)\theta \end{pmatrix}. \tag{17}$$

To summarize, Stress Field II, which generates any displacement field on a flat round plate, has an equibiaxial component described by Eq. (11) and non-equibiaxial components described by Eq. (16) or Eq. (17). If only equibiaxial stress is applied, the resulting height error is described by Eq. (15).

Both Stress Field I and Stress Field II are exact solutions to Eq. (5), which was formulated assuming that no external forces and moments are applied to the substrate (for example, through mounting points). This condition does not necessarily require that the substrate is unmounted. Suppose a set of mounting points each constrain $w(r_i,\theta_i) = 0$, $\partial w(r_i,\theta_i)/\partial x = 0$, and/or $\partial w(r_i,\theta_i)/\partial y = 0$ for each mounting point i. The condition of no external loads will be satisfied if the target deformation, $W(r,\theta)$, is chosen such that it satisfies all of the mounting point constraints. Any constrained displacements in the plane of the substrate may apply in-plane loads, but under the small displacement assumption, these will not affect w.

4. ZERNIKE POLYNOMIAL REPRESENTATION

The surface height of a round plate, especially an optical surface, is often represented using Zernike polynomials, which are functions that form a complete, orthonormal basis set on the unit disk. In this section, we decompose Stress Field II into Zernike polynomials. Representing Stress Field I using Zernike polynomials is messy, but we describe a simple process for calculating the Zernike magnitudes of Stress Field I at the end of this section.

The Zernike polynomials, defined in Eq. (18), each have a radial degree n and azimuthal order m. The Zernike polynomials are each a product of a radial polynomial, $R_n^m(\rho)$, and a sine or cosine function. The radial coordinate is normalized

as $\rho = r/R$. We normalize the magnitude as in Noll [23] such that the RMS value of $Z_n^m(\rho,\theta)$ is 1. Many resources (e.g., Ref. [21]) tabulate the first several orders. The Zernike polynomials are

$$Z_n^m(\rho,\theta) = \sqrt{\frac{2(n+1)}{1+\delta_{m0}}} R_n^m(\rho) \begin{cases} \sin|m|\theta & \text{if } m<0 \,\&\, n \geq |m|, \\ \cos m\theta & \text{if } m \geq 0 \,\&\, n \geq |m|, \\ 0 & \text{otherwise,} \end{cases}$$

$$\text{where } R_n^m(\rho) = \sum_{j=0}^{\frac{n-|m|}{2}} \frac{(-1)^j (n-j)!}{j!\left(\frac{n+|m|}{2}-j\right)!\left(\frac{n-|m|}{2}-j\right)!} \rho^{n-2j}. \tag{18}$$

The Zernike polynomials are harmonic height functions for $n = |m|$ and non-harmonic for $n > |m|$. A visual representation and classification of the Zernike polynomials is shown in Fig. 3. The harmonic functions, as shown in Section 2.B, are not exactly correctable with equibiaxial stress alone. Harmonic functions are also created by attempting to generate any shape with $|m| > 1$ using equibiaxial stress only, according to Eq. (15).

The displacement field we would like to generate is

$$w(r,\theta) = \sum_{m=-\infty}^{\infty} \sum_{n=|m|(2)}^{\infty} \omega_n^m Z_n^m(\rho,\theta), \tag{19}$$

where ω_n^m are constants. The indices on the inner sum may be understood to be $n = |m|, |m|+2, |m|+4, \ldots$.

Using Eqs. (11), (14), and (17), we determine the stress field that generates a displacement composed of a single Zernike polynomial, $w(r,\theta) = \omega_n^m Z_n^m(\rho,\theta)$. Normalizing the radial variable and using $|m|$ where necessary, the stress components become

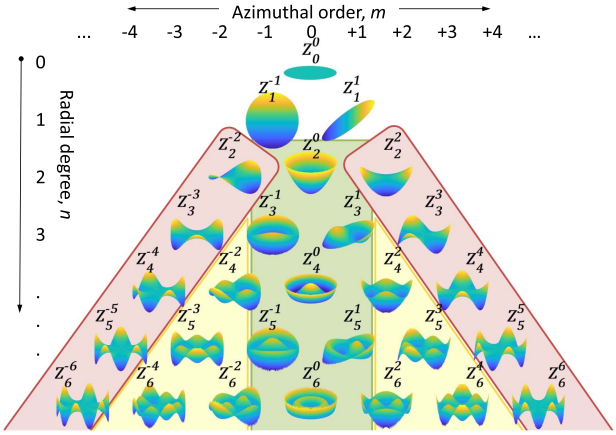

Fig. 3. Zernike polynomials, Z_n^m. The center three columns (green, $|m| \leq 1$) can be corrected with equibiaxial stress only, using Stress Field II. The harmonic components, located on the edge (red, $|m| = n$) cannot be corrected with equibiaxial stress. The remaining components (yellow) can be eliminated with equibiaxial stress but generate harmonic components (red) as described in Eq. (15).

$$(N'_e)_n^m = \omega_n^m \frac{2D}{h_s R^2} \left(\nabla_\rho^2 Z_n^m - (1+\delta_{m0})(1-\nu_s) \frac{\sqrt{|m|-1}}{2} \times \sqrt{n+1} \left[\frac{dR_n^m}{d\rho} - \frac{|m|}{\rho} R_n^m \right]_{\rho=1} Z_{|m|}^m \right),$$

$$(N'_a)_n^m = \omega_n^m \frac{2D(1-\nu_s)}{h_s R^2} \sqrt{1+\delta_{m2}-\delta_{m(-2)}} \frac{\sqrt{|m|-1}}{2} \times \sqrt{n+1} \left[\frac{dR_n^m}{d\rho} + \frac{|m|}{\rho} R_n^m \right]_{\rho=1} Z_{|m|-2}^{\text{sgn}(m)(|m|-2)},$$

$$(N'_s)_n^m = -\omega_n^m \frac{2D(1-\nu_s)}{h_s R^2} \text{sgn}(m) \sqrt{1+\delta_{m(-2)}-\delta_{m2}} \frac{\sqrt{|m|-1}}{2} \times \sqrt{n+1} \left[\frac{dR_n^m}{d\rho} + \frac{|m|}{\rho} R_n^m \right]_{\rho=1} Z_{|m|-2}^{-\text{sgn}(m)(|m|-2)}. \tag{20}$$

Here, $\text{sgn}(m) = \begin{cases} -1 & \text{if } m<0 \\ 1 & \text{if } m \geq 0 \end{cases}$ and ∇_ρ^2 indicate that the radial variable has been normalized in the ∇^2 operator. We may simplify these expressions using the following two identities adapted from Janssen [22]:

$$\left[\frac{dR_n^m}{d\rho} \pm \frac{|m|}{\rho} R_n^m \right]_{\rho=1} = \frac{1}{2}(n \pm |m|)(n \mp |m| + 2),$$

$$\nabla_\rho^2 Z_n^m = \sum_{k=0}^{\frac{1}{2}(n-|m|-2)} [(n+|m|+2k+2)(n-|m|-2k) \times \sqrt{(n+1)(|m|+2k+1)}] Z_{|m|+2k}^m. \tag{21}$$

Using these expressions, we obtain the integrated stress field required to generate a displacement field, $w(r,\theta) = \omega_n^m Z_n^m(\rho,\theta)$, as a function of n and m only. The stress components are

$$(N'_e)_n^m = \omega_n^m \frac{2D}{h_s R^2} \times \sum_{k=0}^{\frac{1}{2}(n-|m|-2)} \left(1 - \delta_{k0} \frac{(1+\delta_{m0})(1-\nu_s)}{4} \right) E_n^m(k) Z_{|m|+2k}^m,$$

$$(N'_a)_n^m = \omega_n^m \frac{2D(1-\nu_s)}{h_s R^2} \sqrt{1+\delta_{m2}-\delta_{m(-2)}} \times E_n^m(k=-1) Z_{|m|-2}^{\text{sgn}(m)(|m|-2)},$$

$$(N'_s)_n^m = -\omega_n^m \text{sgn}(m) \frac{2D(1-\nu_s)}{h_s R^2} \sqrt{1-\delta_{m2}+\delta_{m(-2)}} \times E_n^m(k=-1) Z_{|m|-2}^{-\text{sgn}(m)(|m|-2)},$$

$$\text{where } E_n^m(k) = (n+|m|+2k+2)(n-|m|-2k) \times \sqrt{(n+1)(|m|+2k+1)}. \tag{22}$$

For the arbitrary displacement field defined in Eq. (19), the total stress field is the sum of the stress fields resulting from Eq. (22) for each displacement field component. Each component of the stress field may be represented in terms of the

displacement magnitudes ω_n^m as follows. Here, we use p and q to distinguish between the displacement (n, m) and stress (p, q) components. The stress components are defined as

$$N'_e(r,\theta) = \frac{2D}{h_s R}\sum_{q=-\infty}^{\infty}\sum_{p=|q|(2)}^{\infty}\eta_p^q Z_p^q,$$
$$N'_a(r,\theta) = \frac{2D}{h_s R}\sum_{q=-\infty}^{\infty}\alpha_q Z_{|q|}^q,$$
$$N'_s(r,\theta) = \frac{2D}{h_s R}\sum_{q=-\infty}^{\infty}\sigma_q Z_{|q|}^q, \tag{23}$$

where the constants are

$$\eta_p^q = \frac{\sqrt{p+1}}{R}\left(1-\delta_{p|q|}\frac{(1+\delta_{q0})(1-\nu_s)}{4}\right) \times \sum_{n=(p+2)(2)}^{\infty}\omega_n^q(n+p+2)(n-p)\sqrt{n+1},$$
$$\alpha_q = \frac{1-\nu_s}{4R}\sqrt{(1+\delta_{q0})(|q|+1)} \times \sum_{n=(|q|+2)(2)}^{\infty}\omega_n^{\mathrm{sgn}(q)(|q|+2)}(n+|q|+2)(n-|q|)\sqrt{n+1},$$
$$\sigma_q = \mathrm{sgn}(q)\frac{1-\nu_s}{4R}\sqrt{(1+\delta_{q0})(|q|+1)} \times \sum_{n=(|q|+2)(2)}^{\infty}\omega_n^{-\mathrm{sgn}(q)(|q|+2)}(n+|q|+2)(n-|q|)\sqrt{n+1}. \tag{24}$$

From Eqs. (23) and (24), it is evident that each equibiaxial stress component depends on the displacement magnitudes only within the same column of the Zernike triangle (i.e., $m = q$). The non-equibiaxial components are only composed of those Zernike polynomials on the edges of the Zernike triangle, and they depend on the displacement magnitudes in columns of azimuthal order 2 higher than the stress component.

A potential problem arises since the sums over n in Eq. (24) go to infinity and the value of the summands increases with n. Often, optical surfaces represented by Zernike polynomials will have Zernike magnitudes that decrease with increasing radial degree n. If these magnitudes do not decrease fast enough to compensate for the increase in the value of the summands in Eq. (24), or if the metrology instrument has significant noise in Zernike space, it will be necessary to limit the number of Zernike terms used to represent the surface to avoid a divergent series for the stress field.

Representing Stress Field I as Zernike polynomials is not as clean as for Stress Field II. However, the Zernike components may be determined by calculating the second derivatives of each Zernike component. Noll [23] presents the Cartesian derivatives of Zernike polynomials, which may be codified as

$$\frac{\partial Z_n^m}{\partial x} = \frac{1}{R}\sum_{k=0}^{\frac{1}{2}(n-|m|)}\sqrt{(n+1)(n-2k)} \times \left[\sqrt{1+\delta_{m0}-\delta_{m(-1)}}Z_{n-2k-1}^{m+1}+\sqrt{1-\delta_{m0}+\delta_{m1}}Z_{n-2k-1}^{m-1}\right],$$
$$\frac{\partial Z_n^m}{\partial y} = \frac{1}{R}\sum_{k=0}^{\frac{1}{2}(n-|m|)}\sqrt{(n+1)(n-2k)} \times \left[\sqrt{1+\delta_{m0}+\delta_{m(-1)}}Z_{n-2k-1}^{-(m+1)}-\sqrt{1-\delta_{m0}-\delta_{m1}}Z_{n-2k-1}^{-(m-1)}\right]. \tag{25}$$

The partial derivatives of a displacement field as defined in Eq. (19) may be expressed as a linear combination of Zernike polynomials,

$$\frac{\partial w}{\partial x} = \sum_{q=-\infty}^{\infty}\sum_{p=|q|(2)}^{\infty}\chi_p^q Z_p^q, \qquad \frac{\partial w}{\partial y} = \sum_{q=-\infty}^{\infty}\sum_{p=|q|(2)}^{\infty}\gamma_p^q Z_p^q, \tag{26}$$

where the constants are

$$\chi_p^q = \sum_{n=(p+1)(2)}^{\infty}\frac{\sqrt{(n+1)(p+1)}}{R}\left[\omega_n^{q-1}\sqrt{1+\delta_{q1}-\delta_{q0}} + \omega_n^{q+1}\sqrt{1+\delta_{q0}-\delta_{q(-1)}}\right],$$
$$\gamma_q = \sum_{n=(p+1)(2)}^{\infty}\frac{\sqrt{(n+1)(p+1)}}{R}\left[\omega_n^{-(q+1)}\sqrt{1+\delta_{q(-1)}+\delta_{q0}} - \omega_n^{-(q-1)}\sqrt{1-\delta_{q0}-\delta_{q1}}\right]. \tag{27}$$

The components of the second derivatives may then be calculated numerically by using Eq. (26) twice, and the stress components for Stress Field I may be found using Eq. (9).

5. CORRECTION USING EQUIBIAXIAL STRESS

Making an exact correction of an arbitrary surface height requires applying non-equibiaxial integrated stress components. In Section 1, we listed some methods by which this may be achieved, but it is in any case more challenging to control three stress components than to control one. In addition, many methods of shape correction use equibiaxial stress only. In this section, we use the results from Section 4 to illustrate how much we may improve the original shape error when we are limited to using equibiaxial stress only and how much more stress this requires. This gives us insight to allow us to design a stress field that balances the residual height and the required stress magnitude.

If we can only use equibiaxial stress to make an approximate correction of a surface, we must choose at least one residual height Zernike component for every azimuthal order m present in the original surface height field. For example, if we use Eq. (11) to correct a surface height, we will generate harmonic displacement terms according to Eq. (15). We can then choose an additional stress field to *add* a non-harmonic shape plus a new harmonic displacement field that cancels the generated harmonic displacement field. In effect, we are trading one error

for another. The problem now becomes one of choosing which Zernike components should remain after the correction is made.

The choice of which error components should remain will depend on the available stress magnitude and the components of the original shape, and we will not attempt to find the optimal choice. In this section we will derive expressions for the RMS residual surface height and slopes and the required RMS equibiaxial integrated stress. In Section 6, we will use these relations to design a stress field to approximately correct a measured glass wafer.

Since for $|m| < 2$ we make exact corrections using only equibiaxial stress, we will only consider Zernike displacement terms with $|m| \geq 2$ in this section. We attempt to generate a displacement field composed of a single Zernike polynomial, $w_0 = \omega_n^m Z_n^m$. The error from applying Eq. (11) is Δw_0,

$$\Delta w_0(r,\theta) = -\omega_n^m \frac{(n+|m|)(n-|m|+2)}{4|m|}\sqrt{\frac{n+1}{|m|+1}}Z^m_{|m|}. \tag{28}$$

To remove the residual height Δw_0, we *add* another displacement, $w_1 = \omega^m_{|m|+2j} Z^m_{|m|+2j}$, that results in a displacement $\Delta w_1 = -\Delta w_0$. We designate j as the *radial degree offset*. The residual displacement is

$$w_1(r,\theta) = -\omega_n^m \frac{(n+|m|)(n-|m|+2)}{4(|m|+j)(j+1)}\sqrt{\frac{n+1}{|m|+2j+1}}Z^m_{|m|+2j}. \tag{29}$$

The equibiaxial stress field that results in deformation $w_1(r,\theta)$ may be found using Eq. (22). By the above process, we trade the original shape w_0 for the new shape w_1. We will compare the RMS values of the residual height and slopes for the original and new shapes. We designate RMS quantites with angle brackets $\langle \ldots \rangle$. The RMS height of the new shape, $\langle w_1 \rangle$, may be compared with that of the original shape, $\langle w_0 \rangle$,

$$\frac{\langle w_1 \rangle}{\langle w_0 \rangle} = \frac{(n+|m|)(n-|m|+2)}{4(|m|+j)(j+1)}\sqrt{\frac{n+1}{|m|+2j+1}}. \tag{30}$$

The x- and y-partial derivatives of a Zernike polynomial are given by Eq. (25), and the RMS slopes may be found by calculating the root-sum-of-squares (RSS) of the magnitudes of each component in the derivative expression. For a surface composed of multiple Zernike components, the RSS of the constants of Eq. (27) is equal to the RMS slope in that direction.

Using Eqs. (25), (28), and (29), we calculate the RMS slopes for a choice of radial degree offset j. The RMS slopes in the x and y directions are equal for $|m| \geq 2$, and we designate the RMS slope of the new shape as $\langle s_1 \rangle$ and that of the original shape as $\langle s_0 \rangle$. The ratio is

$$\frac{\langle s_1 \rangle}{\langle s_0 \rangle} = \frac{(n+|m|)(n-|m|+2)}{2\sqrt{2}(|m|+j)(j+1)}\sqrt{\frac{2(j+1)(|m|+j)-|m|}{n^2+2n-|m|^2}}. \tag{31}$$

Equations (30) and (31) indicate that as j increases, both the RMS height and RMS slope errors decrease. We may therefore trade one Zernike component for a higher-degree component to improve these errors. The RMS slope error improves more slowly than the height error. The required RMS equibiaxial stress also increases. These facts are illustrated in Fig. 4 for a particular displacement Zernike term. The results are similar for other Zernike terms.

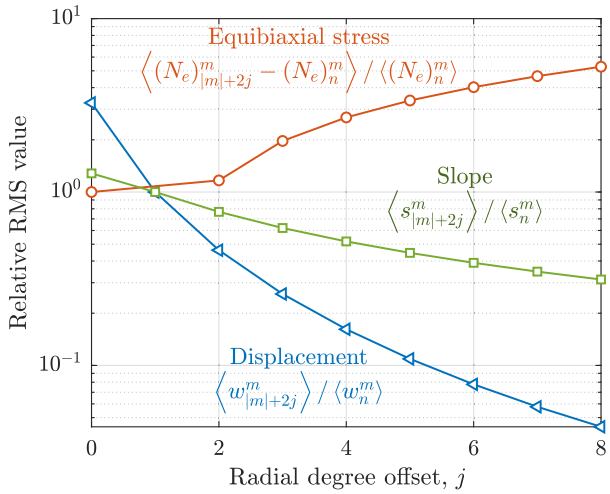

Fig. 4. Improvement in RMS surface height and slope and increase in RMS stress, resulting from trading the original displacement (which is composed of a single Zernike term with $m = -3, n = 5$) for Zernike terms of different radial degrees. This demonstrates one method of designing an equibiaxial stress field to make an approximate correction. Here, the case $j = 1$ involves no applied stress.

6. SIMULATED CORRECTION OF A WAFER

We apply the stress fields in Section 4 and the approximate corrections from Section 5 to simulate the exact and approximate correction (flattening) of a measured glass wafer. We also verify these results using ADINA, a commercial finite element (FE) package. The wafer was measured mounted vertically, using a Shack–Hartmann surface metrology system [25] and a low-stress wafer mounting frame [26]. The measured surface slopes of the wafer are fit to derivatives of Zernike polynomials to obtain the Zernike spectrum of the surface. The surface height map is shown in Fig. 5. The RMS height is 3.64 μm, and the RMS x and y slopes are 10.6 and 9.5 μrad, respectively.

For the simulations in this section, the wafer radius is 50 mm, its thickness is 0.50 mm, and the film thickness is 10 μm. The elastic modulus is 73.6 GPa and the Poisson's ratio is 0.23 for both the substrate and film. The wafer is constrained kinematically so no external loads are applied through the constraints.

We calculate stress fields using each of the three methods: Stress Field I, Stress Field II, and Equibiaxial Only. We apply our analytical stress fields to a finite element model, which is composed of two layers of nine-node shell elements (i.e., quadratic displacement interpolation functions). The top layer is 10 μm thick, and the bottom layer is 500 μm thick. We assume small deformations, small strains, and linear elastic isotropic material properties. We apply a stress field to the top layer. The mesh, composed of 9876 nodes per layer, is shown in

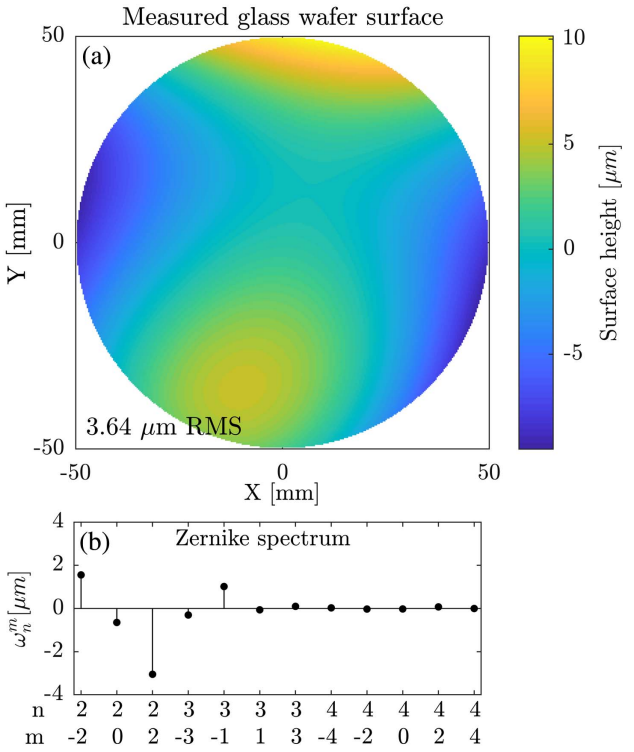

Fig. 5. Measured glass wafer surface. (a) The surface height including Zernike terms up to n=7, and (b) the Zernike spectrum, which is dominated by astigmatism.

Fig. 6. In both the approximate and exact correction cases, the finite element model and analytical model show excellent agreement, as summarized in Table 1. The results do not appreciably change as a result of using a half- or double-density mesh.

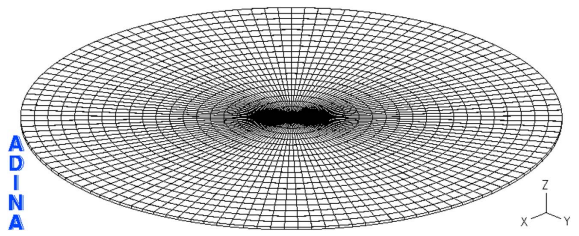

Fig. 6. Finite element mesh used for simulations. This model is composed of two layers of nine-node shell elements bonded together, and an initial stress is applied to the top layer.

Table 1. Residual Height Errors and Stress Field Components Using Three Methods[a]

	RMS Height [nm]		RMS Stress [N/m]		
Method	**Analytic**	**FE**	N_e	N_a	N_s
Stress Field I	0.0	0.0	30.2	18.4	10.0
Stress Field II	0.0	0.8	38.9	14.6	8.0
Equibiaxial only	342.6	342.7	108.4	0.0	0.0

[a]The original RMS height was 3.64 μm.

For exact correction, we apply the Stress Field II components calculated using Eqs. (23) and (24), and the required stress field is shown in Fig. 7. We also use Eqs. (9) and (26) to apply Stress Field I. In both cases, the RMS difference between the analytical and FE models is <1 nm. The RMS lateral displacements are about 50 nm.

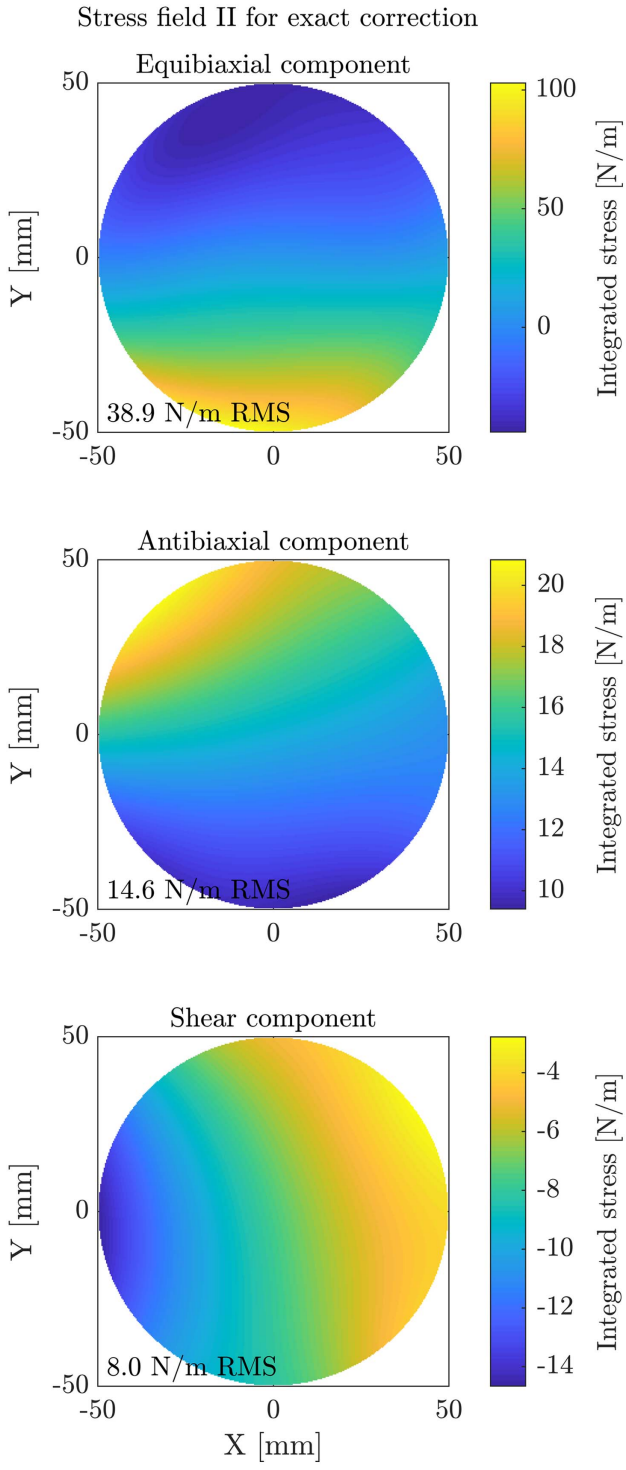

Fig. 7. Integrated stress field, as calculated using Stress Field II, that would exactly flatten the measured glass wafer shown in Figure 5.

For approximate correction using only equibiaxial stress, we know from Section 5 that choosing the residual height error to be higher-order Zernike terms leads to better correction but higher stress requirements. Figure 8 shows this trade-off for this glass surface for a variety of radial degree offset values. For comparison, in Fig. 8 we have also included the RMS values of the stress components required by the general stress field to achieve exact correction.

We arbitrarily chose a radial degree offset value of $j = 2$ and plot the required equibiaxial stress component and corresponding residual height error in Fig. 9. The RMS point-by-point difference between the analytical and numerical model is 8 nm, <0.25% of the total deformation. The RMS residual height error for this radial degree offset value is 343 nm. The RMS lateral displacements are about 50 nm.

Since the deformation is related to substrate thickness, thickness variation could limit accurate correction. We use the finite element model to evaluate the effects of substrate thickness variation by applying Stress Field II to the above substrate but with spatially varying thickness. The target deformation is as in Fig. 5. We describe the small thickness variation

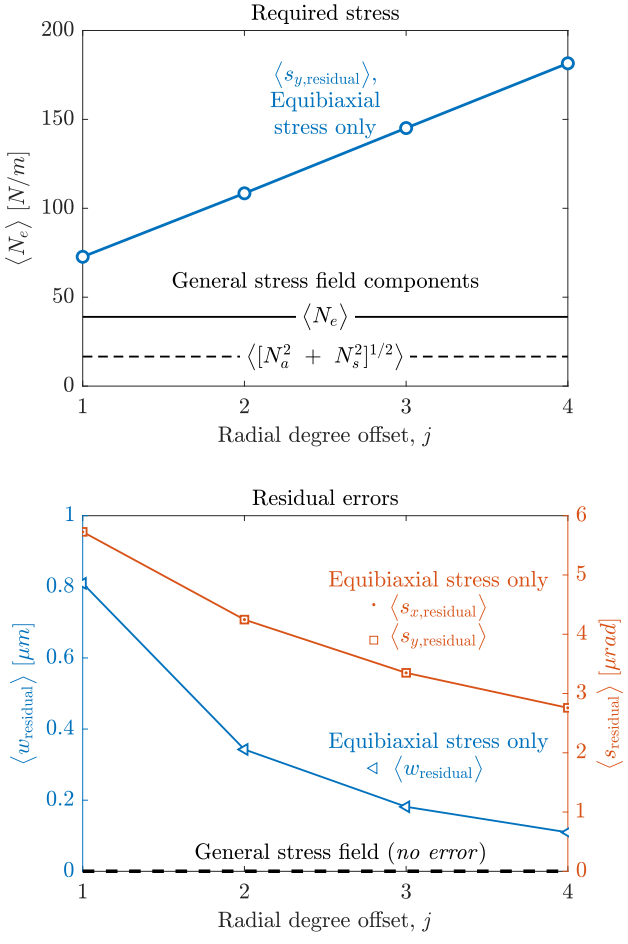

Fig. 8. Increase in required equibiaxial stress (top) and reduction in RMS height and slope errors (bottom) resulting from choosing residual height terms of varying radial degree offset j, as described in Section 5. For comparison, the stress magnitudes calculated using Stress Field II for a full correction are also included.

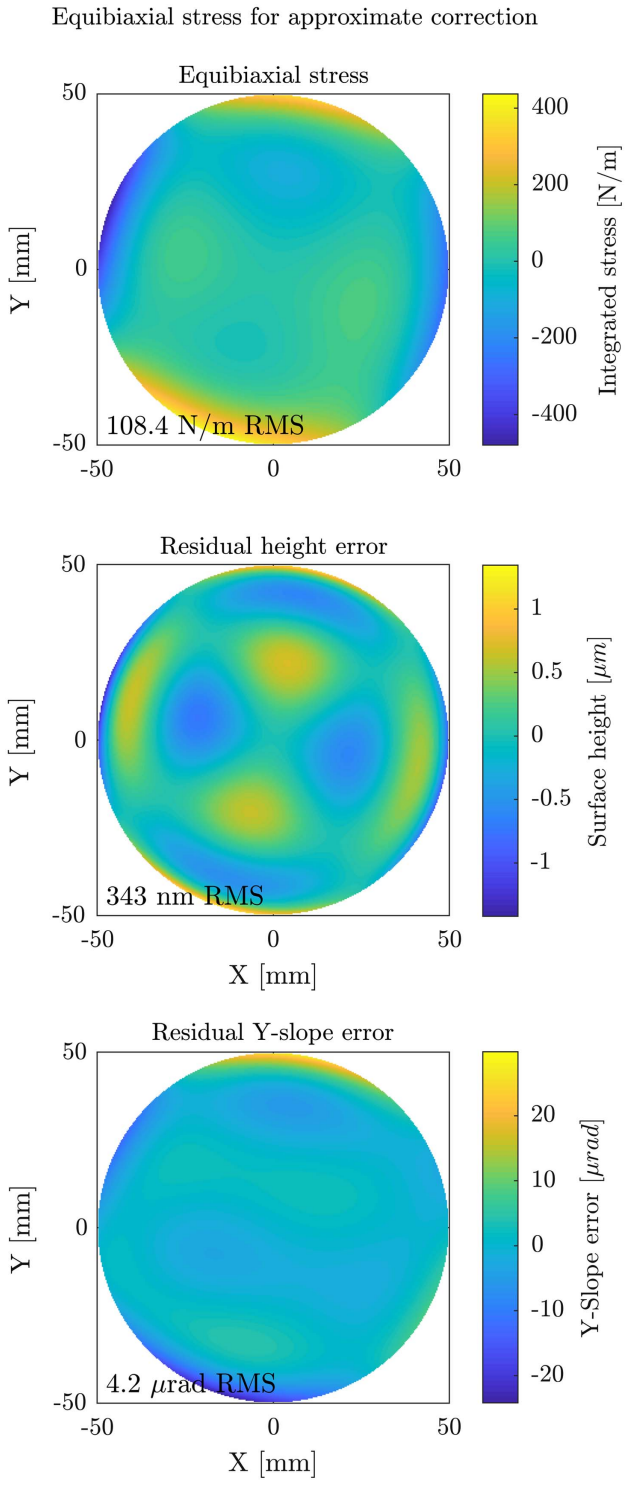

Fig. 9. Equibiaxial stress field, residual height map, and residual slope map in the y direction for $j = 2$. The slope map in the x direction is similar to the slope map in the y direction but rotated 90°, and the RMS value is 4.3 μrad.

$\Delta h_s(r, \theta) \ll h_s$ by a Zernike polynomial with maximum value ±1 μm. To simplify the model definition, the film is initially flat, although in reality it would conform to the substrate. For uniform Δh_s, under this simplification, the expected RMS

Table 2. Residual Height Errors Resulting from Small Variations in the Substrate Thickness $\Delta h_s \ll h_s$

$\Delta h_s(r,\theta)/(-1\ \mu\text{m})$	Z_0^0	$Z_1^1/2$	$Z_2^0/\sqrt{3}$	$Z_3^1/\sqrt{8}$
RMS height error [nm]	20.2	3.5	3.9	1.3

height error is $\langle w - W \rangle \approx 3\Delta h_s/h_s$. The height error resulting from thickness variation is summarized in Table 2. The RMS height error also varies approximately linearly with the thickness variation magnitude, up to at least 50× larger than those in Table 2, and we do not find a significant difference between using Stress Field I and Stress Field II.

7. CONCLUSIONS

For any stress-based figure correction approach being considered, it is important to understand the trade-offs of controlling all three components of surface stress compared to controlling equibiaxial stress only. Controlling one component of stress is of course much simpler than controlling three components. For a flat plate of any shape, however, we have shown that by controlling equibiaxial stress only, we cannot provide an exact correction in general.

We presented two stress fields in Section 3 that may be used to correct an arbitrary surface height error. Stress Field I may be applied to flat plates of any shape. Stress Field II is applicable to round flat plates only, but requires smaller RMS non-equibiaxial stress components than Stress Field I. Stress Field II is compactly represented as a linear combination of Zernike polynomials in Section 4. These two stress fields are not the only solutions, as different choices of constants in Eq. (11) will lead to additional solutions.

Stress Field II may also be used to design a stress field to make an approximate correction using equibiaxial stress only, as described in Section 5. Our approach to approximate correction using only equibiaxial stress is not the only approach, since one may consider having any combination of displacement terms as residual error. The approach we describe illustrates the trade-offs necessary when using equibiaxial stress only.

In practical applications, many complications arise, such as those listed in Section 1. While the stress fields presented here are solutions to an idealized model, they are a useful starting point for further optimization or to account for additional details. One major difference between the idealized model here and most telescope mirrors, for example, is that most telescope mirrors are not flat. Applying the stress fields here to curved plates does not result in a perfect correction. Forthcoming work will address this and other effects.

Funding. National Aeronautics and Space Administration (NASA) (NNX14AE76G, NNX17AE47G); National Science Foundation (NSF) (1122374).

Acknowledgment. The authors thank Youwei Yao, Heng E. Zuo, Brian L. Wardle, Martin L. Culpepper, Lester Cohen, and Will Zhang for valuable discussions.

REFERENCES

1. F. A. Harrison, W. W. Craig, F. E. Christensen, C. J. Hailey, W. W. Zhang, S. E. Boggs, D. Stern, W. R. Cook, K. Forster, P. Giommi, B. W. Grefenstette, Y. Kim, T. Kitaguchi, J. E. Koglin, K. K. Madsen, P. H. Mao, H. Miyasaka, K. Mori, M. Perri, M. J. Pivovaroff, S. Puccetti, V. R. Rana, N. J. Westergaard, J. Willis, A. Zoglauer, H. An, M. Bachetti, N. M. Barrière, E. C. Bellm, V. Bhalerao, N. F. Brejnholt, F. Fuerst, C. C. Liebe, C. B. Markwardt, M. Nynka, J. K. Vogel, D. J. Walton, D. R. Wik, D. M. Alexander, L. R. Cominsky, A. E. Hornschemeier, A. Hornstrup, V. M. Kaspi, G. M. Madejski, G. Matt, S. Molendi, D. M. Smith, J. A. Tomsick, M. Ajello, D. R. Ballantyne, M. Baloković, D. Barret, F. E. Bauer, R. D. Blandford, W. N. Brandt, L. W. Brenneman, J. Chiang, D. Chakrabarty, J. Chenevez, A. Comastri, F. Dufour, M. Elvis, A. C. Fabian, D. Farrah, C. L. Fryer, E. V. Gotthelf, J. E. Grindlay, D. J. Helfand, R. Krivonos, D. L. Meier, J. M. Miller, L. Natalucci, P. Ogle, E. O. Ofek, A. Ptak, S. P. Reynolds, J. R. Rigby, G. Tagliaferri, S. E. Thorsett, E. Treister, and C. M. Urry, "The Nuclear Spectroscopic Telescope Array (NuSTAR) high-energy X-ray mission," Astrophys. J. **770**, 103 (2013).
2. A. Pfahl, J. Coventry, M. Röger, F. Wolfertstetter, J. F. Vásquez-Arango, F. Gross, M. Arjomandi, P. Schwarzbözl, M. Geiger, and P. Liedke, "Progress in heliostat development," Solar Energy **152**, 3–37 (2017).
3. J. A. Gaskin, R. Allured, S. R. Bandler, S. Basso, M. W. Bautz, M. F. Baysinger, M. P. Biskach, T. M. Boswell, P. D. Capizzo, K.-W. Chan, M. M. Civitani, L. M. Cohen, V. Cotroneo, J. M. Davis, C. T. DeRoo, M. J. DiPirro, A. Dominguez, L. L. Fabisinski, A. D. Falcone, E. Figueroa-Feliciano, J. C. Garcia, K. E. Gelmis, R. K. Heilmann, R. C. Hopkins, T. Jackson, K. Kilaru, R. P. Kraft, T. Liu, R. S. McClelland, R. L. McEntaffer, K. S. McCarley, J. A. Mulqueen, F. Özel, G. Pareschi, P. B. Reid, R. E. Riveros, M. A. Rodriguez, J. W. Rowe, T. T. Saha, M. L. Schattenburg, A. R. Schnell, D. A. Schwartz, P. M. Solly, R. M. Suggs, S. G. Sutherlin, D. A. Swartz, S. Trolier-McKinstry, J. H. Tutt, A. Vikhlinin, J. Walker, W. Yoon, and W. W. Zhang, "Lynx Mission concept status," Proc. SPIE **10397**, 103970S (2017).
4. K. Patterson and S. Pellegrino, "Ultralightweight deformable mirrors," Appl. Opt. **52**, 5327–5341 (2013).
5. A. Wirth, J. Cavaco, T. Bruno, and K. M. Ezzo, "Deformable mirror technologies at AOA Xinetics," Pro. SPIE **8780**, 87800M (2013).
6. I. Kanno, T. Kunisawa, T. Suzuki, and H. Kotera, "Development of deformable mirror composed of piezoelectric thin films for adaptive optics," IEEE J. Sel. Top. Quantum Electron. **13**, 155–161 (2007).
7. C. T. DeRoo, R. Allured, V. Cotroneo, E. Hertz, V. Marquez, P. B. Reid, E. D. Schwartz, A. A. Vikhlinin, S. Trolier-McKinstry, J. Walker, T. N. Jackson, T. Liu, and M. Tendulkar, "Deterministic figure correction of piezoelectrically adjustable slumped glass optics," Proc. SPIE **10399**, 103991M (2017).
8. D. Spiga, M. Barbera, A. Collura, S. Basso, R. Candia, M. Civitani, M. S. Di Bella, G. Di Cicca, U. Lo Cicero, G. Lullo, C. Pelliciari, M. Riva, B. Salmaso, L. Sciortino, and S. Varisco, "Manufacturing an active X-ray mirror prototype in thin glass," J. Synchrotron Radiat. **23**, 59–66 (2016).
9. Y. Yao, X. Wang, J. Cao, M. E. Graham, S. Vaynman, S. E. Grogans, Y. Cao, and M. P. Ulmer, "Stress manipulated coating for figure reshape of light weight X-ray telescope mirrors," Proc. SPIE **9603**, 96031J (2015).
10. B. Chalifoux, C. Burch, R. K. Heilmann, Y. Yao, H. E. Zuo, and M. L. Schattenburg, "Using ion implantation for figure correction in glass and silicon mirror substrates for x-ray telescopes," Proc. SPIE **10399**, 103991D (2017).
11. X. Wang, Y. Yao, T. Liu, C. Liu, M. P. Ulmer, and J. Cao, "Deformation of rectangular thin glass plate coated with magnetostrictive material," Smart Mater. Struct. **25**, 085038 (2016).
12. A. Wikström, P. Gudmundson, and S. Suresh, "Thermoelastic analysis of periodic thin lines deposited on a substrate," J. Mech. Phys. Solids **47**, 1113–1130 (1999).
13. E. Hong, S. Trolier-McKinstry, R. Smith, S. Krishnaswamy, and C. Freidhoff, "Design of MEMS PZT circular diaphragm actuators

to generate large deflections," J. Microelectromech. Syst. **15**, 832–839 (2006).
14. G. G. Stoney, "The tension of metallic films deposited by electrolysis," Proc. R. Soc. London, Ser. A **82**, 172–175 (1909).
15. S. Suresh and L. B. Freund, *Thin Film Materials: Stress, Defect Formation and Surface Evolution* (Cambridge University, 2009).
16. D. Ngo, Y. Huang, A. J. Rosakis, and X. Feng, "Spatially non-uniform, isotropic misfit strain in thin films bonded on plate substrates: the relation between non-uniform film stresses and system curvatures," Thin Solid Films **515**, 2220–2229 (2006).
17. Y. Huang, D. Ngo, X. Feng, and A. J. Rosakis, "Anisotropic, non-uniform misfit strain in a thin film bonded on a plate substrate," Interact. Multiscale Mech. **1**, 123–142 (2008).
18. G. Vdovin, O. Soloviev, A. Samokhin, and M. Loktev, "Correction of low order aberrations using continuous deformable mirrors," Opt. Express **16**, 2859–2866 (2008).
19. E. S. Claflin and N. Bareket, "Configuring an electrostatic membrane mirror by least-squares fitting with analytically derived influence functions," J. Opt. Soc. Am. A **3**, 1833–1839 (1986).
20. B. Chalifoux, E. Sung, R. K. Heilmann, and M. L. Schattenburg, "High-precision figure correction of x-ray telescope optics using ion implantation," Proc. SPIE **8861**, 88610T (2013).
21. M. Born and E. Wolf, *Principles of Optics*, 1st ed. (Cambridge University, 1999).
22. A. J. E. M. Janssen, "Zernike expansion of derivatives and Laplacians of the Zernike circle polynomials," J. Opt. Soc. Am. A **31**, 1604–1613 (2014).
23. R. J. Noll, "Zernike polynomials and atmospheric turbulence," J. Opt. Soc. Am. A **66**, 207–211 (1976).
24. S. Timoshenko, *Theory of Plates & Shells* (Mcgraw Hill, 1959).
25. C. R. Forest, C. R. Canizares, D. R. Neal, M. McGuirk, and M. L. Schattenburg, "Metrology of thin transparent optics using Shack-Hartmann wavefront sensing," Opt. Eng. **43**, 742–753 (2004).
26. M. Akilian, C. R. Forest, A. H. Slocum, D. L. Trumper, and M. L. Schattenburg, "Thin optic constraint," Precis. Eng. **31**, 130–138 (2007).